Appl. Phys. A 54, 404–410 (1992)

Applied Physics A Solids and Surfaces

Time-Resolved Spectra of Excited-State Absorption in Er^{3+} Doped $YAlO_3$

M. Pollnau, E. Heumann, and G. Huber

Institut für Laser-Physik, Universität Hamburg, Jungiusstrasse 11, W-2000 Hamburg 36, Fed. Rep. Germany

Received 9 October 1991/Accepted 21 February 1992

Abstract. A pump- and probe-beam technique is used for measuring time-resolved excited-state absorption (ESA) and stimulated-emission (SE) spectra of Er^{3+} doped $YAlO_3$. The Er^{3+} $^4I_{15/2} \rightarrow {}^4F_{7/2}$ transition of the sample is excited at 488 nm by an excimer laser pumped dye laser. The ESA and SE of broadband xenon flashlamp light is monitored between 300 and 860 nm by an optical multichannel analyzer (OMA). The analysis of the experimental results provides information on the effective cross sections σ_{ESA} and σ_{SE} originating from several levels and on the populations of these levels. To our knowledge this represents the first detailed investigation of time-resolved ESA and SE over a broad spectral range in rare-earth doped materials.

PACS: 07.65, 35.00, 42.55 R

Excited-state absorption (ESA) may have considerable influence on the lasing properties of rare-earth doped solid-state materials. ESA is a two-step excitation process which occurs in several rare-earth ions. Because both absorption steps take place within the same single ion, ESA depends linearly on the density of the excited ions. A similar process is up-conversion requiring two neighbouring excited ions. If one ion relaxes to a lower state its energy is used to excite the other ion to an even higher energy level. Therefore up-conversion has a square dependence on the density of the excited ions and becomes significant at high doping concentration.

ESA and up-conversion can be utilized for the generation of visible fluorescence by the absorption of infrared pump photons [1–3]. However, in most cases they also produce undesirable losses. Especially the ESA process either reduces the pump efficiency of solid-state lasers or competes with stimulated emission, decreasing or preventing laser output. This depends on whether the ESA wavelength is in the spectral region of the pump light or the fluorescence [4].

Er^{3+} with its complex energy level scheme, which includes some metastable excited states, gives rise to multiple up-conversion and ESA transitions. On the other hand Er^{3+} is an attractive lasing ion with several laser transitions in the visible and infrared spectral region. Therefore, the knowledge of the ESA transitions and the corresponding cross sections over a wide spectral range is of importance not only for the fundamental understanding of the excitation and depopulation processes, but also for the optimisation of the pump process of Er^{3+} doped laser materials.

ESA effects with respect to laser experiments in Er^{3+} doped materials have been discussed by several authors [3, 5–7]. There have only been two previous reports on ESA spectra of Er^{3+} doped glass fibers including ESA originating from the $^4I_{13/2}$ level [8, 9]. In this paper we report the method and results of measurements of time-resolved ESA spectra after pulsed excitation of Er^{3+} doped $YAlO_3$ in the spectral range between 300 and 860 nm. ESA transitions from the $^4I_{13/2}$, $^4I_{11/2}$, and $^4S_{3/2}$ levels were identified and the corresponding cross sections were determined.

1 Experimental

1.1 Measuring Method

To explain the measuring method of ESA spectra a simple energy level scheme is shown in Fig. 1. The relevant processes which have to be considered are characterized by their cross sections σ_{GSA} (ground-state absorption), σ_{ESA} (excited-state absorption), and σ_{SE} (stimulated emission). $n, n_g(t)$, and $n_e(t)$ are the doping concentration, the time-dependent population densities of the ground state and of all excited levels, respectively:

$$n = n_g(t) + n_e(t) = n_g(t) + \Sigma n_i(t) . \quad (1)$$

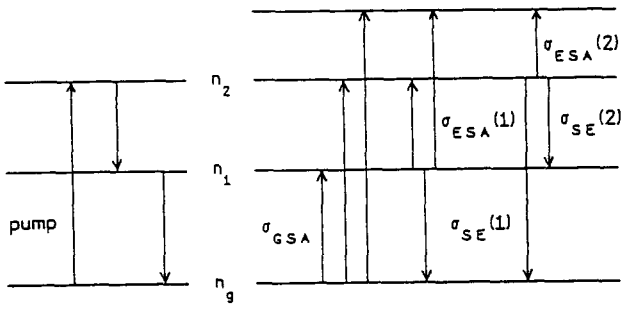

Fig. 1. N-level energy diagram for the explanation of ESA measurements. For clarity only two excited states are shown. Pump excitation, subsequent relaxation (left) and transitions induced by the flashlamp (right) are indicated

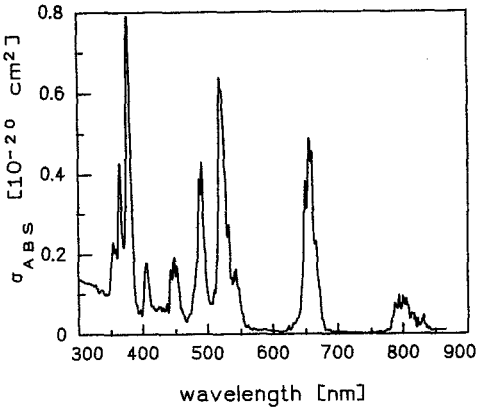

Fig. 2. Absorption spectrum of Er^{3+}:$YAlO_3$. The large spectral linewidths and low cross sections are due to the small spectral resolution (5 nm) available with the set-up for ESA measurements

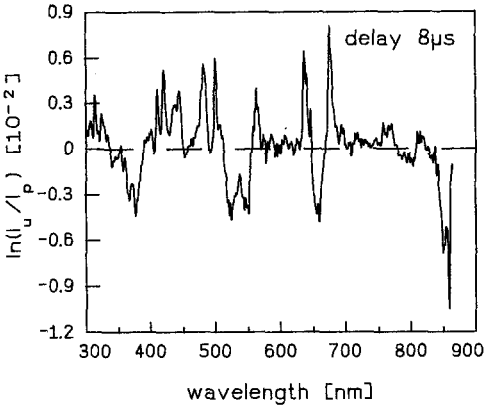

Fig. 3. Spectrum of $\ln(I_u/I_p)$ at 8 μs delay. ESA peaks as well as GSA and SE dips occur

The populations n_i of the excited states are achieved by pumping with a pulsed laser into one level. Subsequent relaxation and up-conversion populates lower and higher lying states. So the sum in (1) generally extends over all populated excited levels. A practical approach is the consideration of all metastable levels because only these levels are substantially populated.

A probe beam of low intensity I_0, such that the populations of the levels are unpertubed, passes through the crystal of length d. In the unpumped case all electrons are in the ground state and the transmitting probe beam intensity is

$$I_u(d) = I_0 \exp(-n\sigma_{GSA} d)\,, \tag{2}$$

whereas in the pumped case it is

$$I_p(d) = I_0 \exp(-d\{n_g\sigma_{GSA} + \Sigma[n_i\sigma_{ESA}(i)] - \Sigma[n_i\sigma_{SE}(i)]\})\,. \tag{3}$$

Dividing (2) by (3) we obtain with (1)

$$\begin{aligned}\ln(I_u/I_p) &= d\{-(n_g + \Sigma n_i)\sigma_{GSA} + n_g\sigma_{GSA} + \Sigma[n_i\sigma_{ESA}(i)] - \Sigma[n_i\sigma_{SE}(i)]\} \\ &= d\{-n_e\sigma_{GSA} + \Sigma[n_i\sigma_{ESA}(i)] - \Sigma[n_i\sigma_{SE}(i)]\}\end{aligned} \tag{4}$$

or

$$\frac{1}{n_e d}\ln(I_u/I_p) + \sigma_{GSA} = \Sigma\left[\frac{n_i}{n_e}\sigma_{ESA}(i)\right] - \Sigma\left[\frac{n_i}{n_e}\sigma_{SE}(i)\right]. \tag{5}$$

To obtain $\sigma_{ESA} - \sigma_{SE}$ the terms on the left hand side of (5) and the populations n_i must be determined. The following steps have to be performed:

1. measurement of the ground-state absorption σ_{GSA},
2. measurement of $\ln(I_u/I_p)$ within the same spectral resolution as in 1.,
3. determination of n_e from the bleaching of the GSA,
4. comparison of ESA peaks at different times after pulsed excitation,
5. calculation of the populations n_i of the metastable levels,
6. calculation of σ_{ESA} and σ_{SE}.

Each of these steps is now explained in detail.

σ_{GSA} is obtained by measuring I_0 and $I_u(d)$ and using (2). The resulting absorption spectrum of Er^{3+}:$YAlO_3$ is shown in Fig. 2. The determination of $\ln(I_u/I_p)$ requires the measurement of four spectra [10]. Each spectrum is labeled by a single letter. The applied beams and the detected signals are qualitatively indicated:

(n) no beam ⇒ dark current,

(t) test or probe beam ⇒ probe beam − GSA + dark current,

(p) pump beam ⇒ fluorescence + scattered pump light + dark current,

(b) both, pump and probe beam ⇒ probe beam $-\left(1 - \frac{n_e}{n}\right)\cdot$ GSA − ESA + SE + fluorescence + scattered pump light + dark current.

The $\left(1 - \frac{n_e}{n}\right)$-term in the (b)-spectrum arises due to the bleaching of the GSA. From these four spectra we compute

$$\ln(I_u/I_p) = \ln[(t-n)/(b-p)]\,. \tag{6}$$

An example of a $\ln(I_u/I_p)$ spectrum at 8 μs after pulsed excitation is shown in Fig. 3. n_e can determined at wavelength regions where GSA but no ESA or SE occurs. For this case we obtain from (5)

$$n_e = \frac{1}{\sigma_{GSA} d}\ln(I_u/I_p)\,. \tag{7}$$

Thus the right hand side of (5) can be calculated. Examples of the resulting spectra at three different delay times are presented in Fig. 5.

The populations n_i of the excited states can be derived from the following considerations: The sum of the absolute populations of all excited states at a certain delay time t_k after pulsed excitation is

$$\Sigma n_i(t_k) = n_e(t_k) \Rightarrow \Sigma \frac{n_i(t_k)}{n_e(t_k)} = 1 . \tag{8}$$

If only the time-depending fraction x_k of the electrons in the metastable excited states is taken into account, then, with N_{ik} being the relative population of level i at delay time t_k, (8) becomes

$$\Sigma \frac{n_i(t_k)}{n_e(t_k)} = \Sigma N_{ik} = x_k \leq 1 . \tag{9}$$

At wavelengths where no SE occurs the time-depending ESA measurements provide the quantities

$$\frac{n_i(t_k)}{n_e(t_k)} \sigma_{\mathrm{ESA}}(i) = N_{ik} \sigma_{\mathrm{ESA}}(i) , \tag{10}$$

as demonstrated in (2)–(5). The comparison of the same ESA peak at different delay times t_1, t_k yields

$$\frac{N_{i1} \cdot \sigma_{\mathrm{ESA}}(i)}{N_{ik} \cdot \sigma_{\mathrm{ESA}}(i)} = \frac{N_{i1}}{N_{ik}} = c_{ik} ,$$
$$i = 1, \ldots, m; \; k = 2, \ldots, m . \tag{11}$$

The measurement of ESA at m different delay times leads to m equations of form (9) and $m(m-1)$ independent equations of form (11). In total m^2 equations allow the determination of the m^2 variables

$$N_{ik}, \quad i, k = 1, \ldots, m . \tag{12}$$

Introducing the abbreviations

$$d_{ik} = (c_{ik} - c_{mk})/(c_{ik} c_{mk}) ,$$
$$e_{ijkl} = d_{ik}/d_{jk} - d_{il}/d_{jl} , \tag{13}$$

the solutions for the relative populations N_{i1} of $m = 3$ excited states, from which ESA originates in Er:$YAlO_3$, can be written as

$$N_{11} = [(x_2 - x_1/c_{32})/d_{22} - (x_3 - x_1/c_{33})/d_{23}]/e_{1232} ,$$
$$N_{21} = -[x_3 - N_{11}/c_{13} + (N_{11} - x_1)/c_{33}]/d_{23} ,$$
$$N_{31} = x_1 - N_{11} - N_{21} . \tag{14}$$

The populations N_{ik} of the levels i at the other times t_k can then be derived from (11):

$$N_{ik} = N_{i1}/c_{ik} . \tag{15}$$

With $n_e(t_k)$ from (7), the absolute populations can be calculated from (10):

$$n_i(t_k) = N_{ik} \cdot n_e(t_k) . \tag{16}$$

Finally, the absolute ESA cross sections $\sigma_{\mathrm{ESA}}(i)$ are obtained from the measured quantity $[n_i(t_k)/n_e(t_k)]\sigma_{\mathrm{ESA}}(i)$ derived from (5). The results are presented in Sect. 2.

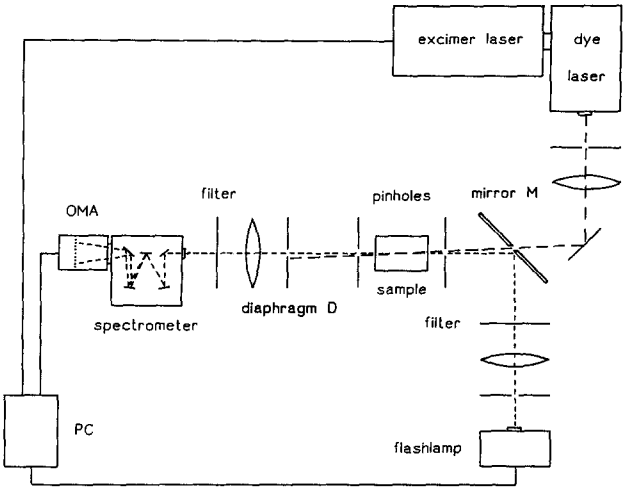

Fig. 4. Experimental set-up for the measurement of time-resolved ESA spectra

1.2 Experimental Arrangement

A pump- and probe-beam technique is used for the time-resolved measurement of ESA spectra. The experimental set-up is shown in Fig. 4. 140 µJ pulses from an excimer laser pumped dye laser (Coumarin 102) at 488 nm are coupled into the sample through the hole in mirror M. The pulse duration of 10 ns is short compared to the lifetimes of the metastable levels of Er^{3+} in $YAlO_3$ and, therefore, a δ-like excitation is realized. The sample is placed between two pinholes of 200 µm in diameter to define an excitation volume. The transmitted pump light is blocked by the diaphragm D or is absorbed by two filters for obtaining spectra which do not overlap with the excitation wavelength. Pulsed white probe light from a xenon flashlamp is focused via mirror M into the sample. The transmitted probe light passes through the diaphragm D into the monochromator. The output spectrum is detected and analyzed with an optical multichannel analyzer (OMA). During the measurement the OMA interface provides regular signals to a pulse and delay generator which generates two pulses. The first pulse triggers the excimer laser and, after an adjustable delay time, the second pulse triggers the flashlamp and gates the OMA detector. The variation of the delay allows the measurement of time-resolved ESA spectra. The minimum delay between excitation and detection of the ESA spectrum is 2 µs. During each measurement four spectra are recorded (see Sect. 1.1). The resulting ESA spectrum is free of scattered pump light and spontaneous fluorescence from the sample.

The ground-state fluorescences at 550 and 966 nm were monitored by a photomultiplier connected to a multichannel analyzer, after pulsed excitation by a N_2 laser pumped dye laser (Coumarin 102) at 488 nm.

2 Results and Discussion

ESA spectra of Er^{3+} doped $YAlO_3$ were measured at several delay times t_k between 2 µs and 10 ms. The sample had a length of 6.9 mm (crystallographic c-axis) and an Er^{3+} concentration of $2.9 \times 10^{20}\,\mathrm{cm}^{-3}$.

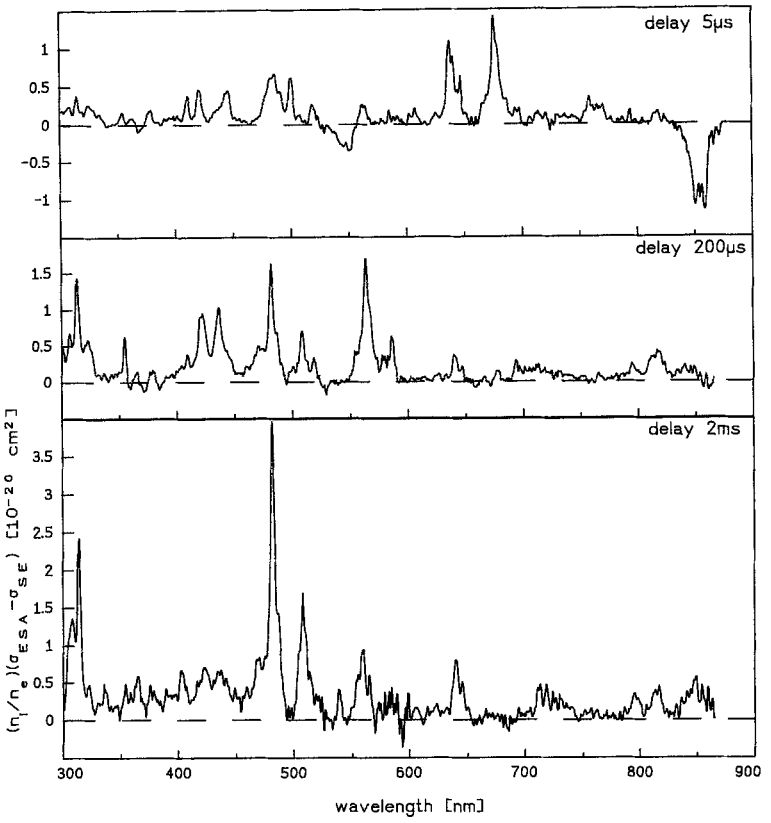

Fig. 5a–c. Spectra of $\sigma_{ESA}(i) - \sigma_{SE}(i)$ times the relative population factor $\frac{n_i}{n_e}$, of Er^{3+}:$YAlO_3$ at 3 different delay times: **a** 5 μs, **b** 200 μs, and **c** 2 ms

Multiple strong ESA has been observed in the entire spectral range between 300 and 860 nm. According to the temporal behaviour of the population and depopulation of the Er^{3+} metastable states after pulsed excitation, the intensities of the ESA peaks vary significantly with delay time. Figures 5a–c show the ESA spectra at three different delay times. The evaluation of the ESA spectra at twelve different delay times (5, 8, 14, 27, 50, 100, 200, 300, 500, 1000, 2000, 3000 μs) results in the identification of three groups of ESA transitions originating from three different levels. Each group exhibits a characteristic temporal behaviour as shown in Fig. 6a. Comparison with the ground-state fluorescence decays from the $^4S_{3/2}$(550 nm) and $^4I_{11/2}$ (966 nm) levels (Fig. 6b) allows the determination of the initial levels of two of these ESA groups. The $^4I_{13/2}$ level has the longest lifetime (6.5 ms), such that at long delay times $n(^4I_{13/2}) \rightarrow n_e$. Therefore, (5) and (10) predict that at long delay times the ESA transitions from the $^4I_{13/2}$ level saturate with the time constant of the $^4I_{11/2}$ level from which the $^4I_{13/2}$ level is mostly populated. This allows the identification of the third ESA group.

It is important to emphasize that the ESA, as well as the fluorescence intensity, is proportional to the absolute population of the initial level. Our evaluation, however, is based on the quantity $(n_i/n_e)[\sigma_{ESA}(i) - \sigma_{SE}(i)]$ which is proportional to the relative population n_i/n_e of the excited level i. The relative and the absolute maximum of the population do not necessarily occur at the same time after excitation. Compare, for example, the absolute and relative populations of the $^4I_{13/2}$ level in Table 1. The absolute population has its maximum at 1 ms, while the relative population is still increasing due to the fast decrease of the excitation of the other levels. So the coincidence of the ESA and fluorescence maxima is not conclusive proof of the origin of the ESA and SE. In this case, however, there is no ambiguity in assigning the ESA data to the ground-state fluorescence data.

Table 1. Absolute (and relative) populations n_i [10^{17} cm^{-3}] of the Er^{3+} metastable states at twelve different times after excitation by 140 μJ pulses from an excimer laser pumped dye laser (Coumarin 102) at 488 nm

Delay time	$^4I_{13/2}$	$^4I_{11/2}$	$^4S_{3/2}$	Excitation
5 μs	1.1 (9%)	1.3 (11%)	9.4 (80%)	11.8 (100%)
8 μs	1.6 (14%)	2.1 (18%)	7.8 (68%)	11.4 (100%)
14 μs	1.7 (16%)	2.5 (23%)	6.6 (61%)	10.8 (100%)
27 μs	1.9 (18%)	3.2 (30%)	5.5 (52%)	10.5 (100%)
50 μs	2.5 (24%)	4.0 (39%)	3.8 (37%)	10.4 (100%)
100 μs	2.9 (28%)	5.4 (52%)	2.0 (20%)	10.3 (100%)
200 μs	3.2 (33%)	5.4 (55%)	1.2 (12%)	9.8 (100%)
300 μs	3.4 (38%)	5.0 (55%)	0.7 (7%)	9.0 (100%)
500 μs	3.4 (43%)	3.9 (50%)	0.5 (7%)	7.8 (100%)
1 ms	3.7 (58%)	2.4 (39%)	0.2 (3%)	6.3 (100%)
2 ms	3.5 (72%)	1.3 (26%)	0.1 (2%)	4.8 (100%)
3 ms	3.0 (80%)	0.7 (20%)	0.0 (0%)	3.8 (100%)

The terminating levels of the ESA transitions originating from the levels mentioned above have been identified by means of the spectral positions of the ESA peaks. Figure 7 shows the energy level scheme of Er^{3+} indicating the observed ESA and SE transitions.

To determine ESA cross sections the populations $n_i(t_k)$ for $m = 3$ levels ($^4S_{3/2}$, $^4I_{11/2}$, $^4I_{13/2}$) were calculated using (14) of Sect. 1.1. The small populations of the other levels were neglected, such that $x_k = 1$ in (9) and (14). It

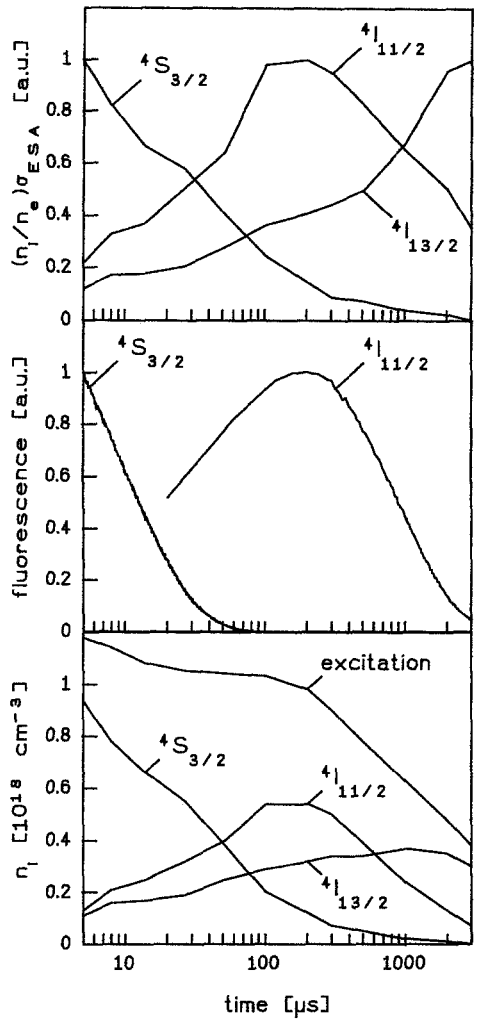

Fig. 6a–c. The temporal behaviour of **a** the ESA peaks originating from $^4S_{3/2}$, $^4I_{11/2}$, and $^4I_{13/2}$, **b** the fluorescences from $^4S_{3/2}$ and $^4I_{11/2}$, and **c** the absolute populations of the metastable levels

must be noted that in (14) the numerator and denominator can equal zero, which may occur if the statistical deviation is too large. Therefore, 4500 spectra of $\ln(I_u/I_p)$ [see (4)] were summed at every delay time for the calculation of the ESA cross sections. The populations of the metastable levels are given in Table 1 and shown in Fig. 6c. The temporal behaviour is in good agreement with that of the fluorescence decays (Fig. 6b). The effective cross sections calculated from these populations are listed in Table 2. Because of the small spectral resolution (5 nm) available, the σ_{ESA} values represent averages over the corresponding Stark multiplets. At the long wavelength side of the spectrum the Stark splitting is partially resolved. The calculated cross sections are not corrected with respect to the Boltzmann populations of the Stark levels because single Stark transitions could not be resolved. Therefore, the $^4S_{3/2} \leftrightarrow {}^4I_{13/2}$ transitions at 840–859 nm have different effective cross sections in SE and ESA (see Table 2). The margin of error is approximately ±20% for the populations as well as the cross sections, and ±2 nm for the wavelengths.

It should be noted that the cross sections of GSA and ESA are of the same order of magnitude. The highest ESA

Table 2. ESA transitions and the corresponding cross sections in $Er^{3+}:YAlO_3$. σ_{ESA} [10^{-20} cm^2] and (λ [nm]) are given

Transition	$^4I_{13/2}$	$^4I_{11/2}$	$^4S_{3/2}$
Unknown			0.7 (411)
Unknown			0.8 (445)
$(^4D)_{7/2}$	1.7 (308)		0.7 (478)
$?_{5/2}$	2.6 (314)		0.6 (491)
			1.0 (500)
$?_{9/2}$	0.6 (337)		
$?_{5/2}$	1.0 (355)	0.7 (408)	0.2 (607)
$(^4G)_{7/2}$	0.7 (366)	1.6 (422)	1.3 (638)
			1.0 (641)
			0.7 (647)
$^2K_{13/2}$	0.6 (378)	2.0 (437)	1.6 (677)
$^2P_{3/2}$	0.6 (403)	0.5 (471)	0.3 (766)
			0.3 (771)
$^2G_{7/2}$	1.0 (471)	2.6 (564)	–
$^2K_{15/2}$		0.5 (574)	–
and	5.1 (482)	0.4 (577)	
$^2G_{9/2}$		1.0 (586)	–
$^4G_{11/2}$	2.1 (508)		–
$^2H_{9/2}$	1.2 (556)	0.4 (694)	–
	1.6 (560)		
$^4F_{3/2}$		0.5 (812)	–
		0.8 (816)	
$^4F_{5/2}$	1.1 (641)	0.3 (833)	–
	0.7 (647)	0.2 (840)	
$^4F_{7/2}$	0.8 (714)	–	–
	0.7 (719)		
	0.5 (725)		
$^2H_{11/2}$	0.7 (795)	–	–
	0.8 (798)		
$^4S_{3/2}$	0.5 (840)	–	–
	0.7 (845)		
	1.1 (849)		
	0.8 (859)		
$^4F_{9/2}$	–	–	–
$^4I_{9/2}$	–	–	–
$^4I_{11/2}$	–	–	–
$^4I_{13/2}$	–	–	0.4 (840)
			0.6 (845)
			1.4 (849)
			1.7 (859)
$^4I_{15/2}$	–	–	0.5 (552)

peak at 482 nm results from the overlap of two transitions. ESA from other levels was not detected because, due to the short liftimes, the populations of these levels are small.

Significant stimulated emission (SE) has been observed on the possible laser transition $^4S_{3/2} \rightarrow {}^4I_{15/2}$ near 550 nm for short delay times after pulsed excitation (see Fig. 5a). The gain vanishes after 100 μs corresponding to the lifetime of the $^4S_{3/2}$ state. On the other hand at longer delay times strong ESA originating from the $^4I_{13/2}$ level is observed in the range 556–560 nm (Fig. 5c). This ESA prevents SE from the $^4S_{3/2}$ level into the upper Stark levels of the $^4I_{15/2}$ level. In addition to the lower emission cross sections at the long wavelength side of the green fluorescence, this effect is the reason why the observed laser action in $YAlO_3$ at low temperatures [3] occurs at 549.6 nm corresponding to the transition into the fourth lowest of eight Stark levels of the ground state. The Boltzmann population of this Stark

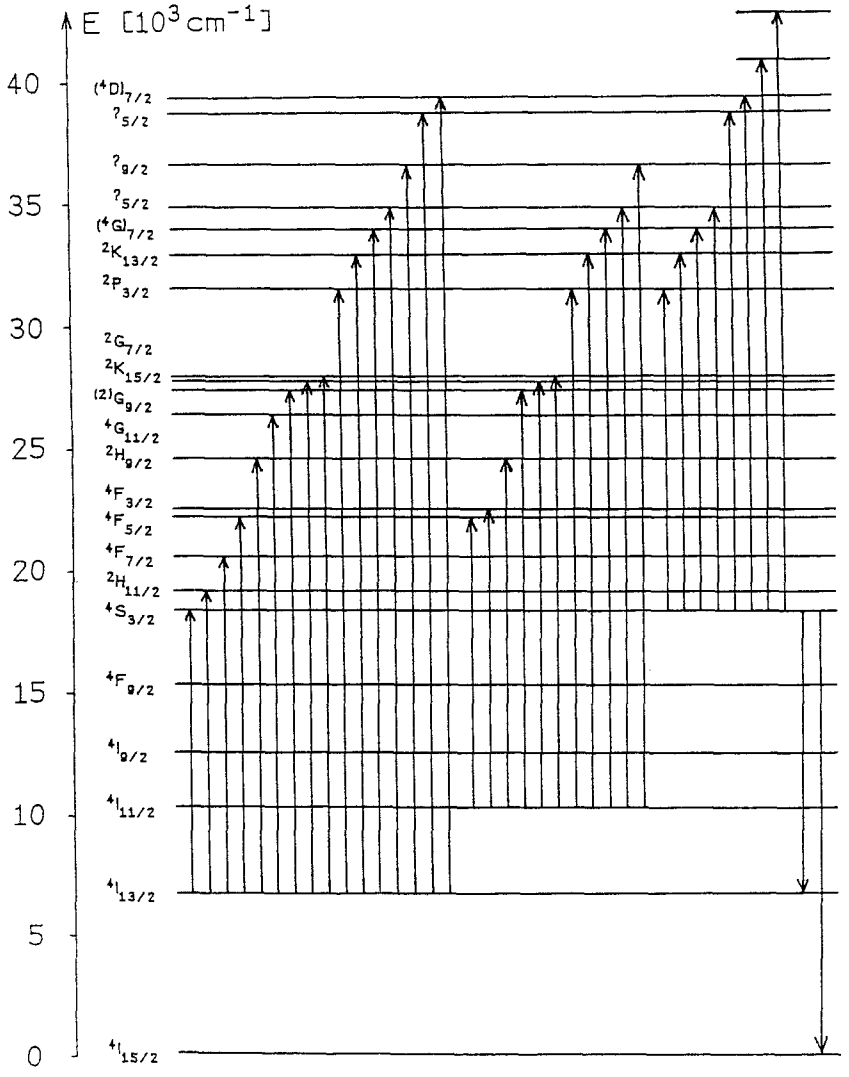

Fig. 7. Energy levels of Er^{3+}:$YAlO_3$ indicating the detected ESA and SE transitions originating from $^4I_{13/2}$, $^4I_{11/2}$, and $^4S_{3/2}$

level does not permit population inversion and stimulated emission under cw excitation at room temperature. The situation for the 850 nm laser transition $^4S_{3/2} \rightarrow {}^4I_{13/2}$ [11] is different. Strong SE occurs at short delay times after excitation (see Fig. 5a). The corresponding population inversion during the first 80 µs can be seen in Fig. 6c. The ESA observed at long delay times (Fig. 5c) is the inverse process $^4I_{13/2} \rightarrow {}^4S_{3/2}$, showing that due to the longer lifetime of the $^4I_{13/2}$ level steady-state inversion can hardly be achieved at room temperature. Figure 6c also shows that inversion on the laser transition $^4I_{11/2} \rightarrow {}^4I_{13/2}$ at 3 µm exists up to 600 µs after pulsed excitation.

The results of the time-resolved ESA measurements clearly show that laser action of Er^{3+}:$YAlO_3$ on both transitions ($^4S_{3/2} \rightarrow {}^4I_{15/2}$ and $^4S_{3/2} \rightarrow {}^4I_{13/2}$) should be possible at room temperature by use of short excitation pulses of a few µs duration.

The wavelength region near 800 nm, which is of importance for diode pumping, contains two ESA transitions at 788–820 nm from the $^4I_{13/2}$ level and at 810–825 nm from the $^4I_{11/2}$ level. The highest peaks occur at 795, 798, 812, and 816 nm. Because GSA at 800 nm ($^4I_{15/2} \rightarrow {}^4I_{9/2}$) is rather small these ESA processes may severely affect the pump efficiency. These ESA transitions may be utilized for up-conversion pumping [3].

Ar^+ and Kr^+ lasers, commonly available in laboratories, are used in laser pumping experiments to optimize the lasing parameters of Er doped materials. The ESA measurements provide the following results: ESA from $^4I_{13/2}$ reduces the pump efficiency at 488 nm. This ESA results in a blue fluorescence from $^2H_{9/2}$. The ESA from the $^4S_{3/2}$ level detected at 491 nm may also extend to 488 nm as was supposed in [7]. However, this cannot be decided from these spectra because of the small resolution available. Krypton laser pumping at 647 nm is influenced by ESA from the $^4I_{13/2}$ and $^4S_{3/2}$ levels. Up-conversion produces green fluorescence from $^4S_{3/2}$ during excitation to any lower lying states, however, after 647 nm excitation to the $^4F_{9/2}$ level the ESA transition $^4I_{13/2} \rightarrow {}^4F_{5/2}$ enhances this fluorescence. There was no ESA measured at the krypton pump wavelength of 521 nm, which is ideal for the excitation of the $^4S_{3/2}$ level.

Finally, previously unknown energy levels of Er^{3+} in $YAlO_3$ where identified by ESA originating from the $^4S_{3/2}$ level at 411 and 445 nm corresponding to transitions into energy levels at 42800 and 40900 cm^{-1} from the ground state.

3 Conclusions

In conclusion, we measured time-resolved ESA spectra of Er^{3+}:$YAlO_3$ ranging from 300 to 860 nm at several delay times from 2 μs to 10 ms. ESA transitions originating from the $^4S_{3/2}$, $^4I_{11/2}$, and $^4I_{13/2}$ levels were identified and their effective cross sections determined. The absolute populations of the excited states were calculated. The influence of the ESA at several pump wavelengths and at the laser wavelengths 550 and 850 nm was analyzed. Laser action on both transitions should be possible at room temperature by use of short excitation pulses of a few μs duration. Two new energy levels at 42800 and 40900 cm^{-1} were identified.

Acknowledgements. We wish to thank H. Stange and T. Danger of the Institute of Laser-Physics, University of Hamburg, Germany, for the development of most parts of the experimental arrangement and for many helpful discussions. We also acknowledge the support of the Deutsche Forschungsgemeinschaft.

References

1. F.A. Auzel: Proc. IEEE **61**, 758 (1973)
2. C. Wright: Topics Appl. Phys., Vol. 15, ed. by K.F. Fong (Springer, Berlin, Heidelberg 1976) p. 239
3. A.J. Silversmith, W. Lenth, R.M. Macfarlane: J. Opt. Soc. A., Vol. 3, 128 (1986)
4. K. Petermann: Opt. Quantum Electron. **22**, S 199 (1990)
5. C.A. Millar, T.J. Whitley: IEE Proceedings, Vol. 137, Pt. J, No. 3, 155 (1990)
6. J. Rubin, A. Brennier, R. Moncorgé, C. Pedrini: J. Lum. **36**, 39 (1986)
7. T. Andreae, D. Meschede, T.W. Hänsch: Opt. Commun. **79**, No. 3, 4, 211 (1990)
8. L. Esterowitz, R. Allen, I. Aggarwil: In Advanced Solid-State Lasers, 1991, Technical Digest Series (Optical Society of America, Washington, DC 1988) p. 160
9. R.I. Laming, S.B. Poole, E.J. Tarbox: Opt. Lett. **13**, No. 12, 1084 (1988)
10. S.A. Payne, L.L. Chase, G.D. Wilke: Phys. Rev. B **37**, No. 2, 998 (1988)
11. S.A. Pollack, D.B. Chang, M. Birnbaum: Appl. Phys. Lett. **54**, No. 10, 869 (1989)